Research paper

Water-soluble inorganic photocatalyst for overall water splitting

Yu Hang Li [a], Yun Wang [b], Li Rong Zheng [c], Hui Jun Zhao [b], Hua Gui Yang [a,*], Chunzhong Li [a,*]

[a] Key Laboratory for Ultrafine Materials of Ministry of Education, School of Materials Science and Engineering, East China University of Science and Technology, 130 Meilong Road, Shanghai 200237, China
[b] Centre for Clean Environment and Energy, Gold Coast Campus, Griffith University, Queensland 4222, Australia
[c] Beijing Synchrotron Radiation Facility, Institute of High Energy Physics, Chinese Academy of Sciences, Beijing 100049, China

ARTICLE INFO

ABSTRACT

In the past 45 years, the search for semiconductors as active photocatalysts for overall water splitting has focused on insoluble materials and their hybrids. An important question is whether soluble semiconductors have the capacity for photocatalysis or similar applications. The dissolved semiconductors will lose the energy band structures for light absorption; however, the undissolved part in saturated solution can still generate electrons and holes under illumination. Unfortunately, this possibility has never been realized. Here we clearly demonstrate the use of a water-soluble sodium molybdate salt as an effective photocatalyst. The material can photocatalyze simultaneously the oxidation and reduction of water under band-gap irradiation. We anticipate that, as a large and traditional class of chemical compounds, the soluble semiconductors may have great potential to be applied in numerous important applications such as catalysis, photovoltaics, light emitting diodes and artificial photosynthesis.

© 2017 Elsevier B.V. All rights reserved.

1. Introduction

The search for suitable photocatalysts for splitting of water into hydrogen (H_2) product is one of the noble missions of material science [1]. One of the critical challenges that must be overcame to enable the practical use in environmental and clean energy areas is finding efficient and stable photocatalysts for overall water splitting (OWS) without sacrificial agents [2,3]. During the past forty years, overwhelming attention has focused on insoluble inorganics (e.g. TiO_2, ZnO and $BiVO_4$), [4–8] insoluble organics (e.g. g-C_3N_4 or other polymers),[9–11] soluble organics (e.g. molecular photocatalysts) [12] and their hybrids as photocatalysts [13–16]. Unfortunately, none of currently reported photocatalysts can be utilized for large-scale applications of H_2 generation [17]. Thus, it is of great importance to expand potential candidates for water splitting field. The soluble inorganics can be dissolved in water, which arises because of the attraction between positive and negative charges, resulting the decomposition of crystalline structures and thus losing energy band structures for light absorption. Noteworthy, more solute added in its saturated solution will remain as crystals, and these undissolved ionic compounds would retain the

geometrical structures for absorbing light and transferring photogenerated carriers. These suggest that the undissolved soluble inorganic semiconductors may represent a new class of photocatalysts for OWS. However, the possible application of soluble inorganic semiconductors as photocatalysts has never been fulfilled, to the best of our knowledge.

Herein, we find a typical soluble inorganic semiconductor, sodium molybdate salt (Na_2MoO_4), as an effective photocatalyst for overall water splitting under band-gap irradiation after precipitating in its saturated solution (see Fig. 1 for schematic mechanism). Experimentally observed results clearly demonstrate the OWS capacity of undissolved Na_2MoO_4 as photocatalyst, recording an apparent quantum yield of 0.36% at 365 nm; whereas the dissolved Na_2MoO_4 solution exhibits no activity. In addition, we present that the undissolved photocatalyst is very stable for OWS for more than two weeks. The findings in this work constitute the first experimental evidence of the capacity of soluble inorganics for photocatalytic OWS, and may hold the promise for the development of soluble inorganics as catalysts for artificial photosynthesis and other scalable technologies that harness solar energy and convert it to fuel.

* Corresponding authors.
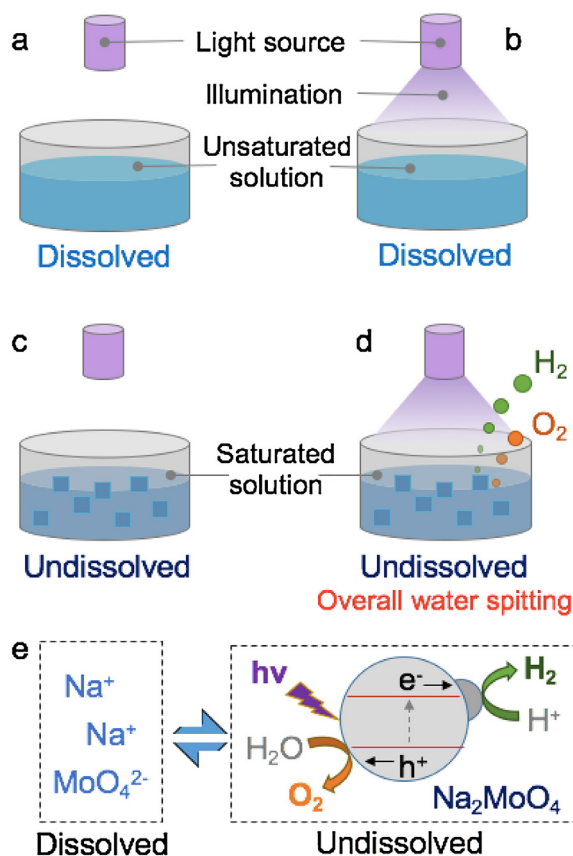   E-mail addresses: hgyang@ecust.edu.cn (H.G. Yang), czli@ecust.edu.cn (C. Li).

Fig. 1. Plausible reaction mechanism of the undissolved Na_2MoO_4 as photocatalyst for overall water splitting. No photocatalytic activity of water splitting can be detected in unsaturated solution in darkness (**a**) or under illumination (**b**), because of the missing energy band structures of the dissolved Na_2MoO_4 sample and the transparency of the solution. No hydrogen or oxygen evolved on undissolved Na_2MoO_4 photocatalyst when the light source was masked (**c**), whereas stoichiometric H_2 and O_2 evolved on undissolved Na_2MoO_4 photocatalyst under illumination (**d**). (**e**) The undissolved ionic compounds would retain the geometrical structures for absorbing light and transferring photogenerated carriers for overall water splitting.

2. Experimental methods

2.1. Synthesis of photocatalyst

In the preparation of the photocatalyst, a two-step synthesis process was involved. Firstly, 1.06 g of commercial Na_2CO_3 (Sinopharm) and 1.44 g of MoO_3 (Sinopharm) was carefully ground, which was carried out in a ball mill with wet grinding method (ethanol, 24 h under rotation speed of 300 r.p.m.). Then we prepared the thermally treated sample through annealing ground mixture in a Muffle furnace at 700 °C for 600 min. The resulting powder can be collected after the furnace cooling down to room temperature. The $Rh_{2-x}Cr_xO_3$ cocatalyst was loaded by an impregnation method. The as-prepared Na_2MoO_4 sample was mixed with an appropriate amount of $RhCl_3$ and $Cr(NO_3)_3$ ethanol solution. Then the suspension was stirred at 80 °C until the liquid was evaporated. After being dried, the mixture was heated in a Muffle furnace at 300 °C for 2 h, and $Rh_{2-x}Cr_xO_3/Na_2MoO_4$ photocatalyst can be collected after the furnace cooling down to room temperature.

2.2. Materials characterizations

The crystal structure was determined using X-ray diffraction (D/MAX 2550 VB/PC). The structure of the catalysts was examined by SEM (S-3400N) and TEM (TECNAI F-30, 300 kV). Brunauer-Emmett-Teller (BET) surface area measurements were performed at 77 K on a Micromeritics ASAS 2460 adsorption analyzer in N_2-adsorption mode. The loading amount of the cocatalyst was tested by ICP-atomic emission spectroscopy (Varian 710 ES). Further, the chemical states of the elements in catalysts were studied by XPS (ESCALAB 250Xi), and the binding energy of the C 1s peak at 284.9 eV was taken as an internal reference. Mo K-edge absorption spectra and in-situ analysis were performed on the 1W1B beamline of the Beijing Synchrotron Radiation Facility (BSRF), China, operated at ~200 mA and ~2.5 GeV. Standard Na_2MoO_4 powder was used as reference sample. A UV torch (365 nm, average intensity of irradiation is about 3.5 mW cm^{-2}) was used in in-situ XAFS analysis to illuminate the unsaturated Na_2MoO_4 solution that in a sealed vessel during the XAFS spectra collection. All samples were measured in the transmission mode.

2.3. Photocatalytic tests

The photocatalytic water splitting tests were carried out in a glass closed-gas-circulation system with a top-irradiation-type reaction vessel (LabSolar H_2). The temperature of the reactant solution was maintained at 20 °C by a flow of cooling water during the tests. A quantity of 1.05 g of photocatalyst that dissolved and precipitated in 10 ml of pure water was added into the reaction vessel for the water splitting test under the illumination of a 365 nm LED. The reactants were sonicated for 10 min for better dispersion and then purged with argon for 5 min to expel the dissolved oxygen. The amounts of evolved hydrogen and oxygen were monitored by an online gas chromatograph (GC-2014C) equipped with a thermal conductivity detector (TCD) and a methanizer and a flame ionization detector (FID) with argon as carrier gas. No air should have remained in the system after evacuation by a vacuum pump. The apparent quantum efficiency (AQE) was measured under the above photocatalytic reaction conditions. It was determined that the average intensity of irradiation was 5.2 mW cm^{-2} and the irradiation area was 12.56 cm^2. The AQE was calculated according to the following equation (see details in Supporting Information):

$$AQE = (number\ of\ reacted\ electrons)/(number\ of\ incident\ photons) \times 100\%$$

$$= (number\ of\ evolved\ H_2\ molecules \times 2)/(number\ of\ incident\ photons) \times 100\%.$$

2.4. Theoretical calculations

All density functional theory (DFT) computations were performed using the Vienna *ab initio* simulation package (VASP) based on the projector augmented wave (PAW) method [18,19]. Electron-ion interactions were described using standard PAW potentials, with valence configurations of $4s^24p^65s^24d^4$ for Mo, $2s^22p^62s^1$ for Na, and $2s^22p^4$ for O. A plane-wave basis set was employed to expand the smooth part of wave functions with a cut-off kinetic energy of 520 eV. For the electron–electron exchange and correlation interactions, the functional parameterized by Perdew-Burke-Ernzerhhof (PBE) [20], a form of the general gradient approximation (GGA), was used throughout. The Na_2MoO_4 crystal was modelled with the primary unit cell including 4 Na atoms, 2 Mo atoms and 8 O atoms. The theoretical lattice constant is 9.290 Å, which is ca. 2% larger than the experimental value. Before the analysis of the electronic properties, the geometry was optimized. All the atoms were allowed to relax until the Hellmann-Feynman forces were smaller than 0.001 eV/Å. The convergence criterion for the electronic self-consistent loop was set to 10^{-5} eV. We performed Brillouin-zone integrations using a gamma-centred $(4 \times 4 \times 4)$ k-point grid for the structural optimization. And a denser

gamma-centred ($8 \times 8 \times 8$) k-point grid was employed for the calculations of DOS and partial charge density of VBM and CBM.

3. Results and discussion

To prepare the Na_2MoO_4 photocatalyst, commercially available Na_2CO_3 and MoO_3 were well grinded with mass ratio of 1.06:1.44 and thermally treated in air to form the Na_2MoO_4 semiconductor with high crystallinity (see details in Methods). Characterizations of the as-prepared sample by scanning electron microscopy (SEM) and transmission electron microscopy (TEM) both show sheet-like particles with an average side length of 5 μm (Fig. S1). The Na_2MoO_4 sample with a d-spacing of 0.52 nm in high-resolution TEM (HRTEM) image corresponds to its (111) crystal faces (Fig. S2) [21]. Moreover, the sample has a surface area of 3.18 $m^2\,g^{-1}$ and an adsorption average pore width of 7.7 nm obtained from Brunauer-Emmett-Teller surface area measurements (Fig. S3). Fig. 2a gives X-ray diffraction (XRD) pattern of the as-prepared photocatalyst, which is assigned well to cubic Na_2MoO_4 bulk (JCPDS Card No. 12-0773). The unit cell of cubic Na_2MoO_4 (a = b = c = 9.108 Å) is shown in the inset of Fig. 2a. It can be seen that Na_2MoO_4 has spinel structure, where Mo atoms occupy tetrahedral (MoO_4) positions in the close packing of oxygen atoms and Na atoms are situated in the octahedral (NaO_6) interstitials. Fig. 2b reports our surface analysis for Na_2MoO_4 sample with X-ray photoelectron spectroscopy (XPS) technique. The deconvoluted Mo 3d doublet peaks suggest that molybdenum is solely in the state of Mo^{6+} (Mo $3d_{5/2}$ = 232.2 eV), and the peaks in the XPS survey scan of the photocatalyst can be only assigned to Na, Mo, O and C elements (Fig. S4), suggesting the inexistence of other elements [22].

In order to know the detailed local atomic structure of Mo atoms, the Na_2MoO_4 photocatalyst was thus characterized by means of Mo K-edge X-ray absorption fine structure (XAFS). The near-edge spectra of the photocatalyst and reference compound Na_2MoO_4 are illustrated in Fig. 2c. The pre-edge peaks in the spectra of these two samples can be attributed to 1s – 4d bound state transition. This transition probability of the formally forbidden excitation is dependent on the local symmetry of Mo atoms [23]. As can be seen in Fig. 2c, only a small decrease of the pre-edge peak of photocatalyst can be observed compared with that of reference Na_2MoO_4, indicating a highly centrosymmetric arrangement around the Mo atom under thermal treatment. The corresponding Fourier-transformed spectra of Mo K-edge extended XAFS (EXAFS) are shown in Fig. 2d. The overlapped peaks in the range of 1–2 Å appear in the curves suggests the comparable atomic structure of the first Mo-O shell between these two samples. Thus, combining with the XRD results, the photocatalyst we prepared has a similar geometrical structure of the bulk Na_2MoO_4 compound.

To understand the electronic structure of Na_2MoO_4 photocatalyst, we calculated the total and partial density of states (DOS) and partial charge density of valence band maximum (VBM) and conduction band minimum (CBM) states using density functional theory (DFT, Fig. 3a). The theoretical band gap energy is 2.64 eV, which is 20% smaller than the experimental value (3.3 eV) detected by the UV–vis absorption spectrum (Fig. 3b) as a result of band gap underestimation within the framework of standard DFT. In addition, the bands close to Fermi energy level are mainly contributed by Mo and O states. DOS and partial charge density plots show that the VBM primarily has O p character, whereas the CBM has Mo 4d and O 2p antibonding character, which suggests electronic structures of Na_2MoO_4 possess dual nature (ionic and covalence). It should be noted that the energies of the CBM and VBM intrinsically determine the reduction and oxidation potentials of photogenerated electron and holes in water splitting [24]. It has been established that VBM of standard Na_2MoO_4 is located at +2.3 eV vs normal hydrogen electrode (NHE) [25], and the similar gap between VBM and Fermi level was confirmed by the XPS valence band spectrum of the sample we prepared (inset in Fig. 3b). Because the band gap of the sample is 3.3 eV from the optical absorption spectrum, the CBM would thus occur at about −1.0 eV vs NHE (Fig. 3c). By comparison with the redox potentials for H^+/H_2 and O_2/H_2O (0 and +1.23 eV vs NHE), clearly, the reduction and oxidation potentials of electrons and holes in Na_2MoO_4 photocatalyst are large enough to achieve OWS.

As a water-soluble semiconductor, the Na_2MoO_4 photocatalyst will be firstly dissolved in water with a solubility of 0.8 $g\,ml^{-1}$, and more added in will remain as crystals (Fig. 4a). The activity of undissolved Na_2MoO_4 photocatalyst for OWS was negligible, which is an analogous phenomenon in many well-studied photocatalysts, such as TiO_2, GaN:ZnO, C_3N_4 and so forth [10,26,27]. Thus, the photocatalyst has been modified with the $Rh_{2-x}Cr_xO_3$ cocatalyst (see details in Methods and Fig. S5) for two reasons as following. (I) The $Rh_{2-x}Cr_xO_3$ cocatalyst has been widely regarded as one of the most effective cocatalysts for pure water splitting on many photocatalysts. In particular, the $(Ga_{1-x}Zn_x)(N_{1-x}O_x)$ photocatalyst that with high AQY for overall water splitting is modified with this cocatalyst [28]. (II) The $Rh_{2-x}Cr_xO_3$ cocatalyst has the capacity for suppress the undesirable backward reaction of water formation from hydrogen and oxygen, which can be easily occurred on most noble metal cocatalysts (such as Pt, Rh, etc.) that have high activity for the half reaction of hydrogen evolution in sacrificial agent [29]. The modification of Na_2MoO_4 with $Rh_{2-x}Cr_xO_3$ cocatalyst resulted in clearly observable H_2 and O_2 evolution, and the solubility of loaded photocatalyst decreases to 0.1 $g\,ml^{-1}$, which may mainly due to the cocatalyst loading. Fig. 4b shows the evolution of H_2 and O_2 from 10 ml of pure water containing 1.05 g of Na_2MoO_4 photocatalyst (0.05 g of precipitation) with the incorporation of 1 wt% $Rh_{2-x}Cr_xO_3$ nanoparticles under band-gap irradiation with a 365 nm LED as light source. The H_2 and O_2 evolution proceeded continuously in a molar ratio of H_2/O_2 of 2.0, which were quantified by an online gas chromatography (GC2014C), effectively identical to the theoretical value of two for OWS, but ceased immediately when the light source was turned off (Fig. 4b). The constant H_2 evolution rate is 1.30 ± 0.10 $\mu mol\,h^{-1}$ and that of O_2 is about 0.65 ± 0.05 $\mu mol\,h^{-1}$, and no other gases can be detected during the reaction (Fig. 4c and Fig. S6). The apparent quantum efficiency (AQE) can be calculated to be 0.36% at 365 nm (see detailed calculations in ESI). Moreover, we found that as the loading content increases, which were tested by inductively coupled plasma (ICP)-atomic emission spectroscopy, the photocatalytic activity increases to a plateau with 1 wt% cocatalyst, beyond which it decreases again (Fig. 4d). Specifically, the photocatalyst would not split water under control experiment when the light source was masked (Fig. 4e). Further control experiments showed that negligible hydrogen gas evolved when $Rh_{2-x}Cr_xO_3$ itself or a mixture of $Rh_{2-x}Cr_xO_3$ and undissolved Na_2MoO_4 as photocatalyst over ten hours (Fig. 4e). The photoluminescence spectra of the bare and cocatalyst modified photocatalysts excited by 340 nm at room temperature (Fig. S7) show an obvious fluorescence quenching at about 375 nm in loaded sample, suggesting the efficiently suppressed radiative charge recombination. [30] These experimental results indicate that the loaded $Rh_{2-x}Cr_xO_3$ cocatalyst is mainly act as H_2 evolution sites on the surface of the undissolved Na_2MoO_4 photocatalyst, and the strong interaction between cocatalyst and host photocatalyst promotes the water splitting to generate H_2 and O_2 significantly.

To determine the possible influence of the dissolved part in this photocatalytic system, the unsaturated Na_2MoO_4 solution was further investigated. The unsaturated solution (10 ml of pure water containing 0.50 g of Na_2MoO_4 photocatalyst with 1 wt% $Rh_{2-x}Cr_xO_3$ as cocatalyst) demonstrated no photocatalytic activity for water splitting illuminated by a 365 nm LED as light source. Moreover,
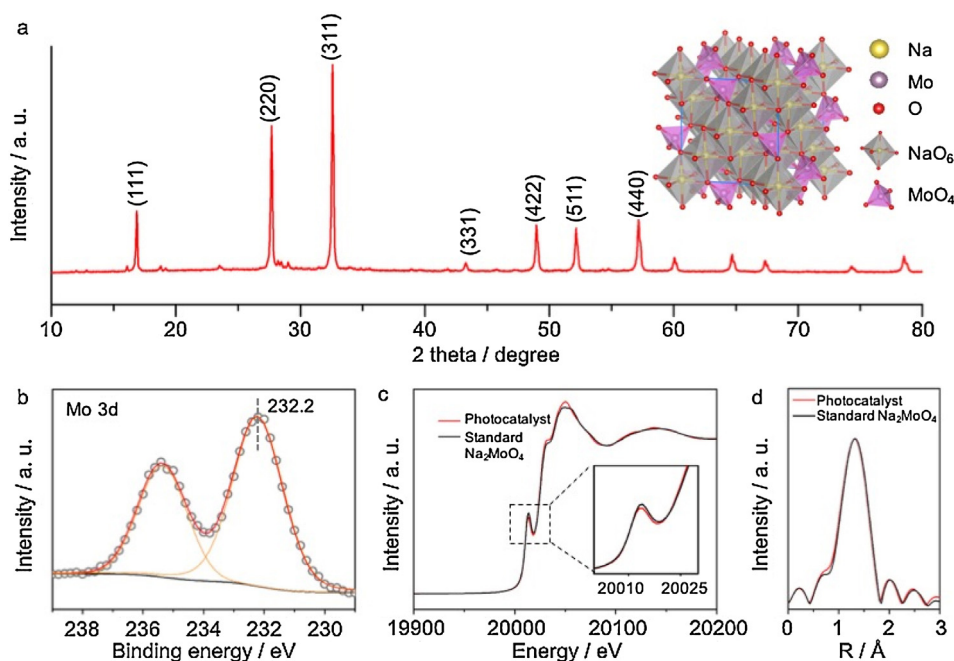
Fig. 2. Structure analyses of the Na_2MoO_4 photocatalyst. (**a**) X-ray diffraction pattern of the Na_2MoO_4 sample we prepared in this work that is in good agreement with the calculated diffraction pattern of cubic Na_2MoO_4. theta, diffraction angle. (**b**) X-ray photoelectron spectroscopy spectra showing the Mo 3*d* core level peak region of the Na_2MoO_4 sample. (**c**) The normalized X-ray absorption near-edge structure spectra at Mo K-edge of our sample and the reference Na_2MoO_4 powder. The inset shows enlarged curves of the pre-edge in the region marked in the figure. (**d**) The k^3-weighted Fourier transform spectra from extended X-ray absorption fine structure.
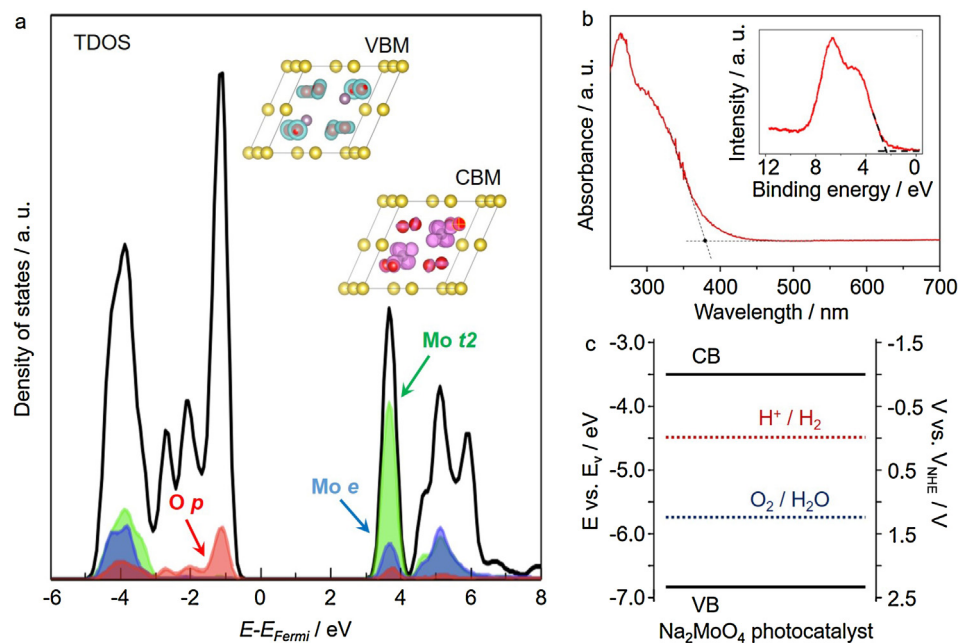

Fig. 3. Electronic structure of the Na_2MoO_4 photocatalyst. (**a**) Calculated densities of states for the unit cell of the Na_2MoO_4 photocatalyst. (**b**) UV–vis absorption spectrum and XPS valence band spectrum (inset in **b**) of the Na_2MoO_4 photocatalyst. The horizontal dashed black line marks the baseline; the other dashed lines are the tangents of the curves. The intersection value is the band gap. (**c**) Band structure diagram for the Na_2MoO_4 photocatalyst. VB, valence band; CB, conduction band.

negligible hydrogen can be detected, even when the methanol as sacrificial agent or $Rh_{2-x}Cr_xO_3$ itself was added in the unsaturated Na_2MoO_4 solution. The results are rationalized in terms of fundamental principles of photocatalysis because of the missing energy band structures of dissolved Na_2MoO_4 and the transparency of unsaturated solution. To further study the possible electronic structure or local atomic structure changes of dissolved sample under band-gap irradiation, the Mo K-edge of above unsaturated

Na_2MoO_4 solution was characterized by using an in-situ XAFS technique (see details in Methods). As presented in Fig. S8, both the near-edge spectra and Mo K-edge EXAFS Fourier-transformed spectra of the unsaturated solution are similar whether under band-gap irradiation or not, suggesting no difference in electron density and local atomic structure of Mo atoms between these two experimental conditions (under irradiation or in darkness). The results obtained from in-situ XAFS analysis display that the dissolved
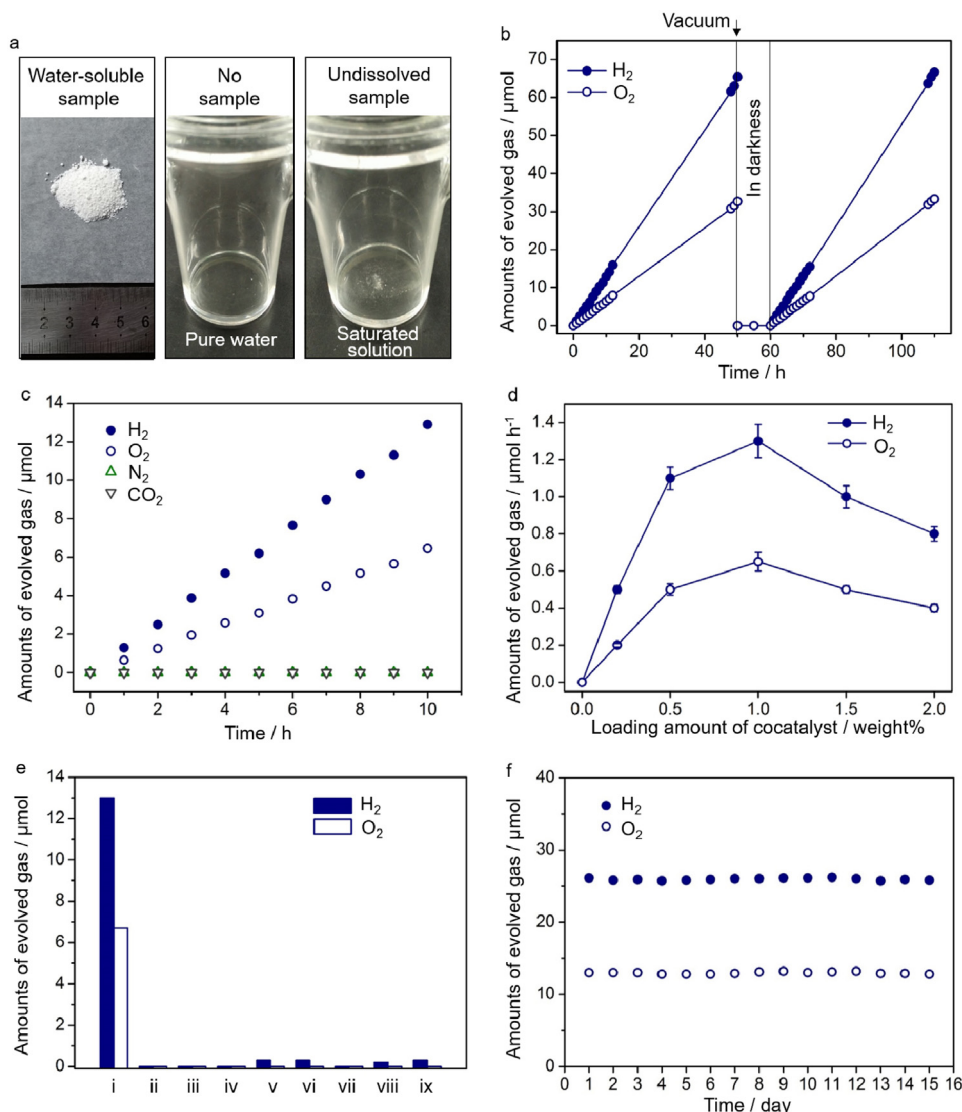
Fig. 4. Photocatalytic tests of the Na_2MoO_4 photocatalyst. (**a**) Digital photos of 1.05 g of Na_2MoO_4 sample, pure water and undissolved sample in photocatalytic reaction vessel (from left to right). Typical time course of H_2 and O_2 production (**b**), and possible N_2 and CO_2 production (**c**) catalyzed by the Na_2MoO_4 photocatalyst with 1 wt% $Rh_{2-x}Cr_xO_3$ cocatalyst under band-gap irradiation. (**d**) Evolution rates of H_2 and O_2 production for different loading contents of $Rh_{2-x}Cr_xO_3$ cocatalyst on Na_2MoO_4 photocatalyst. (**e**) Controlled photocatalytic tests in different experimental conditions. i) 1.05 g of $Rh_{2-x}Cr_xO_3/Na_2MoO_4$ photocatalyst in deionized water under irradiation. ii) No photocatalyst in deionized water under irradiation. iii) 1.04 g of Na_2MoO_4 sample in deionized water under irradiation. iv) 1.05 g of $Rh_{2-x}Cr_xO_3/Na_2MoO_4$ photocatalyst in deionized water in darkness. v) 0.01 g of $Rh_{2-x}Cr_xO_3$ sample in deionized water under irradiation. vi) A mixture of $Rh_{2-x}Cr_xO_3$ (0.01 g) and Na_2MoO_4 (1.04 g) in deionized water under irradiation. vii) 0.50 g of $Rh_{2-x}Cr_xO_3/Na_2MoO_4$ photocatalyst in deionized water under irradiation. viii) 0.50 g of $Rh_{2-x}Cr_xO_3/Na_2MoO_4$ photocatalyst in methanol aqueous solution (20 v/v%) under irradiation. ix) a mixture of $Rh_{2-x}Cr_xO_3$ (0.01 g) and Na_2MoO_4 (0.49 g) in deionized water under irradiation. (**f**) Stability of the undissolved $Rh_{2-x}Cr_xO_3/Na_2MoO_4$ as photocatalyst for water splitting. The amounts of H_2 and O_2 production were collected after 20 h' illumination and the photocatalytic system was evacuated by a vacuum pump in each day. All photocatalytic tests were carried out in a 10 ml of solvent and using a 365 nm LED as light source. The amount of evolved gas in (**e**) was monitored after 10 h' collection.

Na_2MoO_4 solution cannot response to UV light irradiation, indicating its little influence on the activity of undissolved photocatalyst during the water splitting reaction.

Tests have been further conducted to study the stability of the photocatalyst. We found that the activity of OWS was maintained over several cycles for more than two weeks (Fig. 4f), indicating that undissolved Na_2MoO_4 photocatalyst is very stable for repeated cycles without appreciable loss of activity. Specifically, no detectable change has been found in morphology (by scanning electron microscopy) or crystal structure of the Na_2MoO_4 photocatalyst (by X-ray diffraction analysis; Fig. S9). Even the pH values of the solution before and after the stability test stay at the same 8.02. Moreover, the number of moles of product ($\sim$0.4 mmol of H_2) exceeds the number of moles of photocatalyst present ($\sim$0.2 mmol of undissolved photocatalyst), confirming its photocatalytic behav-

ior. These results prove that the undissolved soluble Na_2MoO_4 semiconductor can be used as a photocatalyst for overall water splitting.

4. Conclusions

Unlike all examples in the literatures, we have shown the possibility of using water-soluble Na_2MoO_4 in photocatalytic water splitting, although its high solubility may be a drawback. It has been demonstrated that the undissolved semiconductor indeed has the capacity to absorb light and transfer photogenerated carriers to overall split water under band-gap irradiation for more than two weeks. The performance of this photocatalyst could be further enhanced by refining the preparation method, because the

current high-temperature synthesis would form large particles of Na_2MoO_4. It also appears possible to extend the absorption edge by doping or other energy band engineering methods [31,32]. Our results present that the traditional soluble inorganics offer the prospective development of a new generation of efficient photo-catalysts, and we anticipate that the soluble materials as well as the understanding of mechanism should bring the promise to ful-filment of actual applications in the near future.

Conflict of interest

The authors declare no competing financial interests.

Author contributions

The manuscript was written through contributions of all authors. All authors have given approval to the final version of the manuscript.

Acknowledgments

Appendix A. Supplementary data

Supplementary data associated with this article can be found, in the online version, at http://dx.doi.org/10.1016/j.apcatb.2017.03.001.

References

[1] A. Fujishima, K. Honda, Nature 238 (1972) 37–38.
[2] A. Kudo, Y. Miseki, Chem. Soc. Rev. 38 (2009) 253–278.
[3] X. Chen, S. Shen, L. Guo, S.S. Mao, Chem. Rev. 110 (2010) 6503–6570.
[4] Y.H. Li, J. Xing, Z.J. Chen, Z. Li, F. Tian, L.R. Zheng, H.F. Wang, P. Hu, H.J. Zhao, H.G. Yang, Nat. Commun. 4 (2013) 2500.
[5] C.M. Suarez, S. Hernández, N. Russo, Appl. Catal. A: Gen. 504 (2015) 158–170.
[6] S. Hernández, D. Hidalgo, A. Sacco, A. Chiodoni, A. Lamberti, V. Cauda, E. Tresso, G. Saracco, Phys. Chem. Chem. Phys. 17 (2015) 7775–7786.
[7] T. Jafari, E. Moharreri, A.S. Amin, R. Miao, W. Song, S.L. Suib, Molecules 21 (2016) 900.
[8] K.R. Tolod, S. Hernández, N. Russo, Catalysts 7 (2017) 13.
[9] L.J. Fang, X.L. Wang, Y.H. Li, P.F. Liu, Y.L. Wang, H.D. Zeng, H.G. Yang, Appl. Catal. B: Environ. 200 (2017) 578–584.
[10] J. Liu, Y. Liu, N. Liu, Y. Han, X. Zhang, H. Huang, Y. Lifshitz, S.-T. Lee, J. Zhong, Z. Kang, Science 347 (2015) 970–974.
[11] S. Ghosh, N.A. Kouamé, L. Ramos, S. Remita, A. Dazzi, A. Deniset-Besseau, P. Beaunier, F. Goubard, P.-H. Aubert, H. Remita, Nat. Mater. 14 (2015) 505–511.
[12] A.F. Heyduk, D.G. Nocera, Science 293 (2001) 1639–1641.
[13] L. Zhang, X. He, X. Xu, C. Liu, Y. Duan, L. Hou, Q. Zhou, C. Ma, X. Yang, R. Liu, F. Yang, L. Cui, C. Xu, Y. Li, Appl. Catal. B: Environ. 203 (2017) 1–8.
[14] M. Li, L. Zhang, X. Fan, M. Wu, Y. Du, M. Wang, Q. Kong, L. Zhang, J. Shi, Appl. Catal. B: Environ. 190 (2016) 36–43.
[15] Y.-J. Yuan, Z.-T. Yu, Y.-H. Li, H.-W. Lu, X. Chen, W.-G. Tu, Z.-G. Ji, Z.-G. Zou, Appl. Catal. B: Environ. 181 (2016) 16–23.
[16] K. Maeda, M. Higashi, D. Lu, R. Abe, K. Domen, J. Am. Chem. Soc. 132 (2010) 5858–5868.
[17] J. Xing, W.Q. Fang, H.J. Zhao, H.G. Yang, Chem. Asian J. 7 (2012) 642–657.
[18] G. Kresse, J. Hafner, Phys. Rev. B 47 (1993) 558–561.
[19] G. Kresse, J. Furthmüller, Comput. Mater. Sci. 6 (1996) 15–50.
[20] J.P. Perdew, K. Burke, M. Ernzerhof, Phys. Rev. Lett. 77 (1996) 3865–3868.
[21] X. Liu, Y. Zhao, Y. Dong, Q. Kuang, Z. Liang, X. Lin, D. Yan, H. Liu, Electrochim. Acta 154 (2015) 94–101.
[22] Y.S. Jin, Q.J. Yan, Z.R. Yin, Y. Chen, J. Chem. Soc. Faraday Trans. 91 (1995) 381–384.
[23] R.G. Leliveld, A.J. van Dillen, J.W. Geus, D.C. Koningsberger, J. Catal. 165 (1997) 184–196.
[24] G. Liu, P. Niu, L. Yin, H.-M. Cheng, J. Am. Chem. Soc. 134 (2012) 9070–9073.
[25] S. Rondon, A. Proctor, M. Houalla, D.M. Hercules, J. Phys. Chem. 99 (1995) 327–331.
[26] M. Murdoch, G.I.N. Waterhouse, M.A. Nadeem, J.B. Metson, M.A. Keane, R.F. Howe, J. Llorca, H. Idriss, Nat. Chem. 3 (2011) 489–492.
[27] K. Maeda, T. Takata, M. Hara, N. Saito, Y. Inoue, H. Kobayashi, K. Domen, J. Am. Chem. Soc. 127 (2005) 8286–8287.
[28] T. Hisatomi, J. Kubota, K. Domen, Chem. Soc. Rev. 43 (2014) 7520–7535.
[29] K. Maeda, K. Domen, J. Phys. Chem. Lett. 1 (2010) 2655–2661.
[30] J. Zhang, M. Zhang, R.-Q. Sun, X. Wang, Angew. Chem. Int. Ed. 51 (2012) 10145–10149.
[31] L. Qian, J.F. Chen, Y.H. Li, L. Wu, H.F. Wang, A.P. Chen, P. Hu, L.R. Zheng, H.G. Yang, Angew. Chem. Int. Ed. 54 (2015) 11467–11471.
[32] Z. Zou, J. Ye, K. Sayama, H. Arakawa, Nature 414 (2001) 625–627.